



1 **Molecular fingerprints and health risks of home-use incense burning**
2 **smoke**

3 Kai Song^{1,2,#}, Rongzhi Tang^{3,4,#,*}, Jingshun Zhang⁵, Zichao Wan¹, Yuan Zhang⁶, Kun Hu¹, Yuanzheng
4 Gong¹, Daqi Lv¹, Sihua Lu¹, Yu Tan⁷, Ruifeng Zhang^{3,4}, Ang Li⁸, Shuyuan Yan⁸, Shichao Yan⁸,
5 Baoming Fan⁹, Wenfei Zhu¹⁰, Chak K. Chan^{3,4}, Song Guo^{1,2,*}

6

7 ¹ State Key Joint Laboratory of Environmental Simulation and Pollution Control, International Joint
8 Laboratory for Regional Pollution Control, Ministry of Education (IJRC), College of Environmental
9 Sciences and Engineering, Peking University, *Beijing* 100871, China

10 ² Collaborative Innovation Center of Atmospheric Environment and Equipment Technology, Nanjing
11 University of Information Science & Technology, *Nanjing* 210044, China

12 ³ School of Energy and Environment, City University of Hong Kong, *Kowloon* 999077, Hong Kong,
13 China

14 ⁴ Shenzhen Research Institute, City University of Hong Kong, *Shenzhen* 518057, China

15 ⁵ Shanghai Police College, *Shanghai* 200137, China

16 ⁶ School of Earth Science and Engineering, Hebei University of Engineering, *Handan* 056038, China

17 ⁷ School of Chemical Engineering and Technology, Sun-Yat-Sen University, *Zhuhai* 519000, China

18 ⁸ China Automotive Technology and Research Center (CATARC), *Beijing* 100176, China

19 ⁹ TECHSHIP (Beijing) Technology Co., LTD, *Beijing* 100039, China

20 ¹⁰ School of Energy and Power Engineering, University of Shanghai for Science and Technology,
21 *Shanghai* 200093, China

22

23 # These authors contribute equally to this work.

24 * **Correspondence:** Rongzhi Tang: rongtang@cityu.edu.hk and Song Guo: songguo@pku.edu.cn

25

26

27



28 **Abstract:** The burning of incense for home use is a widespread practice that has been shown to have
29 significant negative impacts on human health and air quality. However, there is a lack of
30 understanding regarding its emission profiles and associated health risks. To address this knowledge
31 gap, we utilized a state-of-the-art thermal desorption comprehensive two-dimensional gas
32 chromatography-mass spectrometer (TD-GC×GC-MS) to (semi-)quantify the emission factors (EFs)
33 of 317 volatile compounds and thoroughly investigate the organic profiles of incense burning smoke
34 across a full-volatility range. Results showed that toluene ($70.8 \pm 35.7 \mu\text{g g}^{-1}$) is the most abundant
35 compound in incensing-burning smoke, followed by benzene, furfural, and phenol. Phenol, toluene,
36 furfural, 2-furanmethanol, benzene, and benzyl alcohol are the main contributors to ozone and
37 secondary organic aerosol (SOA) estimation. Intermediate volatility organic compounds (IVOCs)
38 accounted for 19.2% of the total EFs, but 40.0% of the estimated SOA. Additionally, a novel
39 pixel-based method, combined with aroma analysis, revealed that furfural can act as a key tracer of
40 incense burning, and is responsible for the distinctive flavor of incense smoke. High bioaccumulation
41 potential (BAP) assessment using pixel-based partition coefficient estimation revealed that
42 acenaphthylene, dibenzofuran, and phthalate esters (PAEs) are chemicals of high-risk concern and
43 warrant further control. Our results highlight the critical importance of investigating home-use
44 incense burning and provide new insights into the health impacts of incense burning smoke by novel
45 approaches.

46

47



48 **1 Introduction**

49 Incense burning is a prevalent custom in many cultures, especially in East and Southeast Asia
50 (Chen et al., 2021a). In modern times, incense burning for fragrance has become a frequent partice in
51 households (Manoukian et al., 2013), while functional incense burning, such as mosquito coils, is
52 used for specific purposes. Exposure to incense smoke is linked to adverse health effects like eye
53 irritation, carcinogenicity, genotoxicity, and respiratory system damage (Wong et al., 2020; Yang et
54 al., 2007; Chen et al., 2021b; Yang et al., 2017). Incense is composed of fragrant materials, aromatic
55 woods, herbs, and adhesive powders, usually available in the form of sticks and coils (Wong et al.,
56 2020; Yadav et al., 2022a). Incense burning releases multiple pollutants into the air, including
57 particulate matter (PM), carbon monoxide (CO), volatile organic compounds (VOCs), and
58 intermediate volatility/semi-volatile organic compounds (I/SVOCs) (Wong et al., 2020; Yang et al.,
59 2007; Jetter et al., 2002).

60 Current studies mainly focus on the hazardous VOC and SVOC homologs released from
61 incense-burning smoke. For instance, Lee et al. investigated 8 carbonyls and 11 VOCs emitted from
62 incense burning and found that the emission factors (EFs) of traditional incense burning were higher
63 than aromatic incense (Lee and Wang, 2004). Lu et al. detected 230 kinds of VOCs from
64 mosquito-repellent incense burning, elucidating that alkanes, esters, aldehydes, ketones, and
65 aromatics are predominant (Lu et al., 2020). Staub et al. measured 6 methoxy phenolics, 10
66 monoterpenoids, and other 21 kinds of SVOCs in the burning smoke of incense sticks, and identified
67 cedrol as an important odor source (Staub et al., 2011). However, most of the studies have focused on
68 VOC compounds, with less attention given to gaseous organics in the full volatility range
69 (VOC-IVOC-SVOCs). A full-volatility organic characterization may better evaluate the ozone
70 formation potential (OFP) and SOA formation, as I/SVOCs are potentially important precursors of
71 ozone and secondary organic aerosol (SOA) formation (Lu et al., 2018a; Zhao et al., 2007; Tang et
72 al., 2021a). Meanwhile, mapping organics from incense smoke helps to evaluate the potential health
73 risks of toxic compounds.

74 Comprehensive two-dimensional gas chromatography (GC×GC) is a powerful technique dealing
75 with the coelution problem in conventional one-dimensional gas chromatography (1D GC).



76 Pollutants from gasoline exhaust, diesel exhaust, and cooking emissions are well separated and
77 identified (Drozd et al., 2019; Alam et al., 2018; Song et al., 2022a). As much as 50 ~ 98% of the
78 total response in GC×GC chromatograms could be explained (Huo et al., 2021; Song et al., 2022b).
79 Previous work identified 324 compounds from incense smoke by coupling solid-phase
80 microextraction (SPME) with GC×GC, yet chemicals are not quantified (Tran and Marriott, 2007).
81 Thus, a non-targeted and quantitative assessment of incense burning emissions is currently lacking.

82 In this work, two types of incense sticks and three kinds of incense coils were burned in a steel
83 chamber. Gaseous pollutants were trapped by Tenax TA desorption tubes and then analyzed by a
84 thermal desorption comprehensive two-dimensional gas chromatography-mass spectrometer
85 (TD-GC×GC-MS). Pixel-based multiway principal component analysis (MPCA) was utilized to
86 identify markers of incense burning. Risk assessment of pollutants from incense burning emissions
87 was then evaluated by pixel-based approaches and high-risk compounds related to incense burning
88 were assessed.

89 **2 Methodology**

90 **2.1 Sampling and instrumentation**

91 Incenses were purchased from the market, including 4 common incense sticks, 2 Thailand
92 incense sticks, 1 mosquito coil, and 2 incense coils (Figure S1). Incenses could also be classified by
93 their material, containing 2 aromatic coils, 4 aromatic sticks, 1 mosquito coil, 1 sandalwood stick,
94 and 1 smokeless sandalwood stick (Figure S1). Incenses were burned in a stainless combustion
95 chamber (1 m³). After ignition, the burning incense changed from flaming to smoldering. Each kind
96 of incense was burned at least twice. Incenses were weighed before and after combustion.
97 Preconditioned Tenax TA desorption tubes (Gerstel 6 mm 97 OD, 4.5 mm ID glass tube) were
98 utilized to trap organics with a sampling flow of 0.2 L min⁻¹.

99 A comprehensive two-dimensional gas chromatography-quadrupole mass spectrometer
100 (GC×GC-qMS, GC-MS TQ8050, Shimadzu, Japan) coupled with a thermal desorption system (TDS
101 3 C506, Gerstel, Germany) was used for sample analysis. The desorption temperature was 280 °C.
102 The cooled injection system (CIS) with a Tenax TA liner was held at 20 °C and ramped to 320 °C
103 once injecting the gaseous sample into GC columns. The column combination was SH-Rxi-1ms (1st,



104 30 m × 0.25 mm × 0.25 μm) and BPX50 (2nd, 2.5 m × 0.1 mm × 0.1 μm). The modulation period was
105 6s. See Table S1 and elsewhere (Song et al., 2022a) for more information.

106 **2.2 Chemical identification, quantification, and 2D binning**

107 A series of standard mixtures (2 μg mL⁻¹, 5 μg mL⁻¹, 10 μg mL⁻¹, 20 μg mL⁻¹, 40 μg mL⁻¹ in
108 CH₂Cl₂) was injected into Tenax TA tubes (2 μL). After purging the solvent with nitrogen gas, the
109 standards were thermally desorbed. The standard mixture contains 26 *n*-alkanes (C7 - C32, CNW
110 Technologies, ANPEL Laboratory Technologies (Shanghai) Inc., China), 16 PAHs, 11 phenolic
111 compounds, 9 alcohols, 4 aldehydes, 8 aromatics, 24 esters, 7 ketones, 5 siloxanes, and 39 other
112 compounds. Gaseous organics are quantified by external calibration curves with most of the R²
113 between 0.95 and 0.999 (Table S2). Chemicals with the same retention times and mass spectrums
114 were directly qualified and quantified. The unidentified chemicals were qualified by matching their
115 mass spectrum with library spectrums in the National Institute of Standard Technology library (NIST
116 17). Reverse factors of more than 700 were acceptable in this work. As homologs on the
117 two-dimensional chromatogram (contour plot) were eluted with near-equal one-dimensional intervals,
118 chemicals were then qualified by combing the location of the contour plot and the mass spectrums
119 (Song et al., 2023). Compounds without standards were semi-quantified by *n*-alkanes from the same
120 volatility bin (uncertainty 69%) and surrogates from the same chemical class (uncertainty 27%).
121 Instrument detection limits (IDLs) for organics semi-quantified were unknown, as a result, chemicals
122 with negative values calculated by calibration curves were quantified by the volume-to-mass (ng)
123 ratio of the lowest quantification point of standards (Table S2). A total of 317 chemicals were
124 (semi)-quantified, including 10 acids, 34 alcohols, 19 aldehydes, 25 aromatics, 38 esters, 49 ketones,
125 18 *n*-alkanes, 26 nitrogen-containing compounds, and 10 phenols (Table S3).

126 The compounds identified were sliced into two-dimensional bins (2D bins) (Song et al., 2022a).
127 1st retention times are linked to the volatility of species (B8 to B31 with decreasing volatility) while
128 2nd retention times are associated with polarity (P1 to P8 with increasing polarity). Emission factors
129 of compounds in the same 2D bin were aggregated (Table S3).

130 **2.3 Emission factor (EF), ozone formation potential (OFP), and secondary organic aerosol** 131 **(SOA) estimation**



132 The emission factor (EF, $\mu\text{g g}^{-1}$) was calculated by the following equation:

133
$$EF = \frac{mV}{ftM} \quad (1)$$

134 m is the absolute mass of pollutants (μg) captured by Tenax TA tubes. V is the volume of the
135 steel chamber (1 m^3). The sampling flow and duration of the Tenax TA tube are f ($0.0002 \text{ m}^3 \text{ min}^{-1}$)
136 and t (min), respectively. M is the combustion mass (g) of the incense. The sampling volume of
137 Tenax TA tubes ($0.003 \sim 0.01 \text{ m}^3$) was significantly smaller than the total volume of the steel
138 chamber (1 m^3) and the volume change of the chamber could be neglected.

139 The ozone formation potential (OFP, $\mu\text{g g}^{-1}$) was calculated using equation (2). Where EF_i is the
140 emission factor of precursor i ($\mu\text{g g}^{-1}$) with maximum incremental reactivity (MIR) of MIR_i . The
141 OFP was calculated inside the FOQAT packages developed by Tianshu Chen
142 (<https://github.com/tianshu129/foqat>). The MIR used in this work can be found in Table S3.

143
$$OFP = \sum[EF_i] \times MIR_i \quad (2)$$

144 Secondary organic aerosol (SOA) was estimated by equation (3).

145
$$SOA = \sum[EF_i] \times (1 - e^{-k_{OH,i} \times [OH] \times \Delta t}) \times Y_i \quad (3)$$

146 Where $k_{OH,i}$ and Y_i represent the OH reaction rate and SOA yield of precursor i ,
147 respectively (Table S3). The SOA yields of precursors were from literature (Loza et al., 2014; Harvey
148 and Petrucci, 2015; Tkacik et al., 2012; Shah et al., 2020; McDonald et al., 2018; Chan et al., 2010,
149 2009; Wu et al., 2017; Li et al., 2016; Matsunaga et al., 2009; Algrim and Ziemann, 2019, 2016; Liu
150 et al., 2018; Charan et al., 2020) or surrogates from n -alkanes in the same volatility bins (Zhao et al.,
151 2014a, 2017). k_{OH} and Y could be found in Table S3. $[OH] \times \Delta t$ is the OH exposure and was set to
152 be $13 \times 10^{10} \text{ molecules cm}^{-3}\text{s}$ (24 hours in OH concentration of $1.5 \times 10^6 \text{ molecules cm}^{-3}$).

153 **2.4 Pixel-based risk assessments of incense-burning pollutants**

154 Octanol-air partition coefficient (K_{o-a}), air-water partition coefficient (K_{a-w}), and octanol-water
155 partition coefficient (K_{o-w}) were estimated by a linear free-energy relationship (LFER) model (Nabi
156 et al., 2014; Zushi et al., 2019). Partition coefficients of chemicals are associated with their
157 two-dimensional retention times (Song et al., 2022b). Chemicals with high bioaccumulation potential
158 (BAP) are defined as contaminants with partition coefficients of ($2 < \log K_{o-w} < 11$) and ($6 < \log K_{o-a}$
159 < 12). See Zushi et al. (Zushi et al., 2019) for more information. The R source code was obtained



160 from GitHub (<https://github.com/Yasuyuki-Zushi>).

161 **3 Results and discussions**

162 **3.1 Emission profiles of different incense-burning organics**

163 Figure S2 is a typical chromatogram of incense burning emissions, which is also set as the
164 reference chromatogram during the pixel-based analysis. As much as 90.2% of the total percent
165 response could be explained. The ratio is similar to a recent study resolving biomass burning
166 emissions (98%) (Huo et al., 2021). The emission factor (EF) of total organics is $791.8 \pm 300.6 \mu\text{g g}^{-1}$,
167 consistent with previous work ($100 \sim 19100 \mu\text{g g}^{-1}$) (Lee and Wang, 2004), and comparable to rice
168 ($475.9 \pm 61.2 \mu\text{g g}^{-1}$), pine ($558.6 \pm 103.6 \mu\text{g g}^{-1}$) and poplar ($564.6 \pm 124.1 \mu\text{g g}^{-1}$) combustions
169 (Zhu et al., 2022), but much lower than coal combustion (6.3 mg g^{-1}) (Huo et al., 2021). The
170 contributions of different chemical categories are displayed in Figure S3. Oxygenated compounds
171 dominate the total EFs, accounting for 48.4%, followed by aromatics (29.8%), *b*-alkanes (5.3%),
172 nitrogen-containing compounds (4.0%), alkenes (4.0%), and *n*-alkanes (2.3%). Unresolved complex
173 mixtures (UCMs) are further separated into aliphatic, cyclic, and oxygenated UCM due to retention
174 times and mass spectrums. The UCM ratio in this work (2.3% in EFs) is comparable to biomass
175 burning (Huo et al., 2021) and diesel exhaust (He et al., 2022) analyzed by GC×GC-MS, and is much
176 smaller than the UCM ratio (>50%) in biomass burning smoke analyzed by 1D GC-MS (Zhu et al.,
177 2022). Ketones are the most abundant oxygenated compounds, accounting for 13.6% of the total EFs,
178 followed by aldehydes (9.7%), esters (8.1%), alcohols (6.9%), phenols (3.6%), and acids (3.1%). The
179 emission profiles are comparable to corncob and wood combustion, which are also dominated by
180 ketones and esters (Huo et al., 2021). However, the abundance of phenol is much lower than in
181 biomass-burning smoke (>15%) (Zhu et al., 2022; Huo et al., 2021), while comparable to coal
182 combustion (5.4%) (Huo et al., 2021).

183 EFs of selected compounds are listed in Table S4, which were comparable with other incense
184 burning studies (Lee and Wang, 2004; Yang et al., 2007; Manoukian et al., 2016), while the EF of
185 benzene ($59.6 \pm 43.1 \mu\text{g g}^{-1}$) is slightly lower than other studies ($188 \sim 1826 \mu\text{g g}^{-1}$) (Lee and Wang,
186 2004; Yang et al., 2007; Manoukian et al., 2016). The Tenax TA liner in the CIS system does not
187 capture benzene at an initial temperature of 20 °C, while it is efficient for the trapping of most



188 I/SVOC compounds. Lower CIS temperature may trap benzene while causing water condensation.
189 As a result, the tailing of benzene on the second column (Figure S2) causes an underestimation of
190 blob integration and results in an underestimation of EF.

191 The top 10 compounds are all VOC compounds (Figure S4), accounting for 35.3% of the total
192 EFs. Toluene ($70.8 \pm 35.7 \mu\text{g g}^{-1}$) is the most abundant compound in incensing-burning smoke,
193 followed by benzene, furfural, phenol, styrene, 2-oxo-propanoic acid methyl ester,
194 3-methyl-2-butanone, ethylbenzene, 1-hydroxy-2-propanone, and benzyl alcohol. Note that VOC
195 compounds discussed here are part of volatile organics captured by Tenax-TA, not the common
196 VOCs detected by SUMMA-GC-MS. The top 5 IVOCs are B17 *b*-alkanes, B16 *b*-alkanes, B18
197 *b*-alkanes, diethyl phthalate, and 1,6-dioxacyclododecane-7,12-dione. The naphthalene (a typical
198 PAH, 2 rings) EF is $3.0 \pm 1.5 \mu\text{g g}^{-1}$, comparable to rice straw combustion (Zhu et al., 2022). SVOCs
199 are all *n*-alkane species and only account for less than 1% of the total EFs.

200 The average VBS distribution of incense burning is displayed in Figure 1, and the
201 volatility-polarity distribution is exhibited in Figure S5. In general, the EF decreases as the volatility
202 decreases, following the trend of VOC-EF (80.8%) > IVOC-EF(19.2%) >> SVOC-EF (<0.1%). The
203 chemical compositions in the VOC-IVOC range are shown in Figure S6. Oxygenated compounds
204 (53.5% of the total VOC EFs) and aromatics (37.6%) are largely detected in the VOC range, while
205 *b*-alkanes, *n*-alkanes, and oxygenated compounds are the main components of IVOC compounds.
206 The average VBS distribution is similar to cooking emissions (Song et al., 2022a) and wood
207 combustion (Stewart et al., 2021), but less volatile than gasoline exhausts (Lu et al., 2018b) and more
208 volatile than diesel emissions (Lu et al., 2018b). For example, the proportion of chemicals with
209 saturated vapor concentration (C^*) more than $10^6 \mu\text{g m}^{-3}$ (Figure 1 a) is 80.8% (incense burning),
210 80.7% (cooking emissions) (Song et al., 2022a), 77.6% (wood combustion) (Stewart et al., 2021),
211 94.2% (gasoline exhaust) (Lu et al., 2018b), and 41.0% (diesel exhaust) (Lu et al., 2018b). The
212 polarity of incense burning is dominated by non-polar and intermediate-polarity organics (P1 ~ P5,
213 Figure S5). The volatility-polarity distribution of incense burning is quite similar to cooking
214 emissions (Song et al., 2022a), dominant by VOCs in the volatility range of before B13 and the
215 polarity range of P1 ~ P5.



216 A similar emission pattern but different EFs of different incense-burning emissions are observed.
217 Similarities among incense burning are more dominant than diversities. First, pixel-based partial
218 least squares-discriminant analysis (PLS-DA) elucidates that there is no systemic difference between
219 different chromatograms of incense burning emission, no matter different incense shapes (Figure S7)
220 or materials (Figure S8). Second, the compositions of different types of incense emissions are indeed
221 quite similar (Figure S9 and Figure S10). Third, the multiway principal component analysis (MPCA)
222 positive loadings are much larger than negative loadings, indicating that the similarities between
223 samples are much more important than the differences (Figure 2).

224 However, the absolute EFs significantly diverge according to different incense forms ($p = 0.03$,
225 Figure S11) and different materials ($p < 0.01$, Figure S12). Incense made in stick form (incense stick:
226 $893.2 \pm 335.6 \mu\text{g g}^{-1}$, Thailand incense stick: $877.5 \pm 123.8 \mu\text{g g}^{-1}$) emits more organics than made in
227 coil form (incense coil: $835.5 \pm 306.0 \mu\text{g g}^{-1}$). The EF of mosquito coil is the smallest (382.5 ± 175.0
228 $\mu\text{g g}^{-1}$). A similar pattern was observed in previous work (Jetter et al., 2002). Concerning the incense
229 materials, we spot that the so-called smokeless sandalwood stick emits more abundant organics
230 ($1195.8 \pm 83.3 \mu\text{g g}^{-1}$) than common sandalwood sticks ($633.7 \pm 6.6 \mu\text{g g}^{-1}$). The emission of
231 smokeless sandalwood sticks is even greater than aromatic sticks ($893.2 \pm 335.6 \mu\text{g g}^{-1}$) and coils
232 ($824.8 \pm 228.5 \mu\text{g g}^{-1}$). Our results demonstrate that although smokeless sandalwood stick is
233 preferred as fewer particulates are generated during the combustion process, the gaseous emissions
234 are enhanced compared to other incenses.

235 3.2 Contributions of home-use incense burning to ozone and secondary organic aerosols 236 (SOA)

237 The total OFP is $1513.4 \pm 551.0 \mu\text{g g}^{-1}$ which is $1.91 \text{ g O}_3/\text{g VOC-IVOCs}$. The OFP
238 enhancement ratio (OFP per mass of precursor) is much smaller than gasoline exhaust ($3.53 \text{ g O}_3/\text{g}$
239 VOCs) (Wang et al., 2013) and evaporation ($2.3 \sim 4.9 \text{ g O}_3/\text{g VOC}$) (Yue et al., 2017), showing that
240 incense burning is less efficient on ozone formation than gasoline-related sources. The lack of IVOC
241 measurements in previous work could also cause an overestimation of the OFP enhancement ratio as
242 IVOCs are less efficient in ozone formation. Toluene, furfural, *p*-xylene, benzyl alcohol, phenol,
243 2-furanmethanol, *o*-xylene, ethylbenzene, 1-hydroxy-2-propanone, and benzene are top 10 species



244 that contribute most to OFP (Figure S4). Oxygenated compounds take up 48.2% of the total OFP,
245 followed by aromatics (41.0%), and alkenes (6.7%) (Figure S3). VOCs dominate the total OFP,
246 accounting for 92.4% while IVOCs take up 7.6% (Figure 1). Aromandendrene, naphthalene, and
247 α -cedrene are the top 3 IVOC-OFP contributors. The volatility distribution of OFP contribution is
248 comparable to cooking emissions, as VOCs account for 88.8 ~ 99.9% of the total cooking OFP
249 estimation (Song et al., 2022a). Toluene contributes the most OFP in both cooking emissions and
250 incense burning. Short-chain linear aldehydes (pentanal, hexanal, nonanal) originating from the
251 degradation of oils play a more important role in OFP contribution in cooking emissions (Song et al.,
252 2022a), while benzenes, furfural, alcohols, and phenols are non-negligible OFP contributors in
253 incense burning.

254 Figure 1 shows the volatility distribution of estimated SOA estimation, with the top 10
255 contributors displayed in Figure S4. IVOCs contribute 19.2% of the EFs while accounting for 40.0%
256 of the total SOA estimation, highlighting the importance of IVOCs in SOA formation. The
257 contribution of IVOC species to SOA is higher than EFs due to the relatively higher yields and k_{OH} ,
258 which has already been reported in cooking emissions (Song et al., 2022a; Yu et al., 2022), gasoline
259 exhaust (Zhao et al., 2014b; Tang et al., 2021b), diesel exhaust (Zhao et al., 2015), and biomass
260 burning (Stewart et al., 2021). Oxygenated compounds account for 32.9% of the SOA estimation,
261 followed by aromatics (23.7%), and *b*-alkanes (11.5%) (Figure S3). Phenol, benzyl alcohol, styrene,
262 toluene, B18 cyclic UCM, aromandendrene, 2-furanmethanol, B17 *b*-alkanes, benzene, and
263 phenylethyne are the top 10 SOA contributors. The incense-burning SOA formation profiles are
264 distinct from cooking emissions (Song et al., 2022a) and biomass burning (Huo et al., 2021).
265 Cooking SOA is largely derived from the oxidation of short-chain acids and aromatics (Song et al.,
266 2022a), while phenols account for more than 65% of the SOA estimation from biomass burning (Huo
267 et al., 2021). Phenols only account for 11.0% of SOA estimation in this work. Alcohols (7.3%) and
268 furans (7.6%) are much more important SOA precursors in incense burning compared to biomass
269 burning and cooking emissions. Compared with other sources, we stress the importance of
270 incense-burning benzenes, furfural, alcohols, and phenols in OFP formation and alcohols and furans
271 in SOA formation. The secondary formation potential of mosquito coils is the lowest, while OFP and



272 SOA of burning smokeless sandalwood sticks are the highest. Compared to other incense, the higher
273 aromatic contents of smokeless sandalwood sticks burning fumes result in much more ozone and
274 SOA formation.

275 **3.3 Identification of molecular markers from incense burning**

276 Pixel-based MPCA is utilized to identify tracers of incense burning emissions. In brief, MPCA
277 decomposes a matrix X into a scoring matrix (S) and a loading matrix (L). Similarities and
278 differences in chromatograms are revealed by positive and negative loadings, respectively (Figure 2)
279 (Song et al., 2022b). The similarities of chromatograms could be explained by benzenes (toluene,
280 *p*-xylene, *o*-xylene, and ethylbenzene), ketones (3-methyl-2-cyclopenten-1-one,
281 2-hydroxy-2-cyclopenten-1-one, 3-ethyl-2-pentanone), aldehydes (furfural, succindialdehyde,
282 2-methyl-2-butenal), 2-methyl-propanoic acid, 1-methyl-1H-pyrazole, 2(5H)-furanone, and
283 2-furanmethanol. The differences between samples could be largely explained by 2-methyl-2-butenal,
284 2(5H)-furanone, 3,4-dimethylfuran, 2,3-dihydro-1H-inden-1-one, 2-methoxy-naphthalene, and
285 1,2-dihydro-2,2,4-trimethyl-quinoline. The negative loadings (0.006) are significantly smaller than
286 the positive loadings (0.07), confirming the dominance of similarities among chromatograms. The
287 relationship between the EFs of these compounds among different incense types is displayed in
288 Figure S13. Although the total EFs are significantly different ($p = 0.03$), the EFs of selected
289 compounds (2-hydroxy-2-cyclopenten-1-one, 2-furanmethanol, 3-ethyl-2-pentanone, and furfural are
290 significantly no different ($p > 0.08$). As a result, we recommend these compounds as incense-burning
291 tracers. It is reported that furfural is formed during the thermal degradation of hemicelluloses (Uhde
292 and Salthammer, 2007), while the oxidation of furfural under harsher conditions forms
293 2(5H)-furanone (Depoorter et al., 2021a). The formation mechanism of furfural from xylose and
294 D-xylopyranose is displayed in Figure S14 (Ahmad et al., 1995; Bonner and Roth1, 1959; Nimlos et
295 al., 2006). The initiation of the degradation of five-carbon sugars is from the acyclic form of pentoses
296 or directly via a 2,3-(α,β)-unsaturated aldehyde. The dehydrating of the intermediate compounds
297 finally forms furfural (Figure S14). The addressed tracers, furfural, 2-furanmethanol, and
298 2(5H)-furanone, have already been identified in incense burning smoke in previous work (Depoorter
299 et al., 2021a; Tran and Marriott, 2007).



300 Furthermore, we compare the chemical profiles with an odor database (Aroma Office 2D,
301 Gerstel). Among the top 20 chemicals contributing to EFs, furfural (bread-like, alcoholic,
302 incense-like), phenol (mushroom, acid, burnt plastics), 1-hydroxy-2-propanone (buttery, caramellic,
303 fruity), benzyl alcohol (burning taste, flower, roasted), limonene (citrus-like, fruity, lemon-like), and
304 2-methyl-propanoic acid (apple-like, cheese-like, sweat) could be the aroma compounds. As for
305 tracers identified above, 2-furanmethanol (burnt sugar, honey, sweet) could also be another aroma
306 compound. Among them, furfural is widely and largely detected which could be the most important
307 molecular marker of incense burning (Silva et al., 2021; Depoorter et al., 2021b; Ho and Yu, 2002).
308 Note that aromandendrene, a cucumber-like, woody, and floral compound, is only detected in one
309 incense coil sample (incense coil 2, Figure S1). Aromandendrene is also detected in plants, such as in
310 dry flowers of *Lonicera japonica* (Shang et al., 2011). The emission factor of aromandendrene is
311 rather large ($4.3 \mu\text{g g}^{-1}$, 0.7% of the total EFs), and is a significant SOA precursor ($2.3 \mu\text{g g}^{-1}$, 3.9%
312 of the total SOA estimation). The importance of aromandendrene on incense flavor and SOA
313 formation could not be neglected. Aromandendrene could also be responsible for the distinct flavor
314 of a certain incense coil. As above said, we recommend furfural be used as a molecular indicator of
315 incense burning regardless of the incense type or additives, especially responsible for the flavor of
316 incense burning.

317 **3.4 Risk assessment of incense burning organics**

318 The hazardous compounds from incense burning could cause adverse health effects on human
319 health (Wong et al., 2020; Yang et al., 2007; Chen et al., 2021b; Yang et al., 2017). To evaluate the
320 potential risks of these compounds, we conducted a pixel-based risk assessment (bioaccumulation
321 potential, BAP) for partition coefficient estimation. Chemicals with high BAP concerns are listed in
322 Figure 3. 2-methoxy-naphthalene, acenaphthylene, dibenzofuran, diethyl phthalate, dibutyl phthalate,
323 benzoic acid 2-ethylhexyl ester, C15 – C19 *n*, and *b*-alkanes are regarded as high BAP concern
324 (Figure 3). Among them, acenaphthylene is a toxic polycyclic aromatic hydrocarbon (PAH) that is
325 widely detected in incense smoke (Yadav et al., 2022a). Dibenzofuran, an oxygenated compound
326 with detrimental effects on human health (Suzuki et al., 2021), is also detected in the smoke of
327 incense burning (Tran and Marriott, 2007). Diethyl phthalate and dibutyl phthalate are phthalate



328 esters (PAEs) widely used as plasticizers which are endocrine disruptors (Wang and Qian, 2021).
329 PAEs are abundant in incense smoke (Tran and Marriott, 2007). We propose that acenaphthylene,
330 dibenzofuran, and PAEs could be chemicals of high-risk concern in incense smoke. We also assess
331 the arctic contamination potential (ACP) as shown in Text S1. Further epidemiologic studies should
332 be carried on to demonstrate the health effect of these hazardous compounds.

333 **4 Implication**

334 The non-target approach of GC×GC-MS gives us a full glimpse of incense smoke, spotting a
335 large pool of organics (317 compounds) covering the VOC-IVOC-SVOC range. We have provided a
336 detailed description of both primary emission and secondary estimation of incense burning organics
337 which is ready-to-use in SOA simulation models. IVOCs (130 compounds) are crucial organics
338 accounting for 19.2% of the total EFs and 40.0% of the SOA estimation, highlighting the importance
339 of incorporating IVOCs into SOA models. Further investigation should be carried on to elucidate
340 emission characteristics of short-chain compounds that are lacking in our research, such as alkanes
341 (<C7), alkenes (<C7), and aldehydes (<C5). By combining data obtained from
342 gas-chromatography-flame ionization detector (GC-FID) and proton transfer mass spectrometer
343 (PTR-MS), the emission pattern of incense burning could be well demonstrated. High-time
344 resolution measurement should also be carried on to understand the time-resolved pattern of incense
345 burning.

346 We also suggest furfural as the molecular marker of incense burning as the EFs of furfural
347 among samples are relatively stable. Pixel-based MPCA also indicates that furfural is responsible for
348 the similarities between chromatograms. Furfural may be the key aroma compound of incense smoke.
349 This key component identified in this work could be implemented in source apportionment. Furfural
350 is also a key component contributing to OFP (rank 2). Phenol, toluene, 2-furanmethanol, benzene,
351 and benzyl alcohol are the main contributors to both OFP and SOA.

352 Surprisingly, we find that the EF of burning smokeless sandalwood sticks is the highest, with a
353 remarkable contribution to OFP and SOA, due to the high aromatic contents. We recommend that
354 both gaseous and particulate organics should also be taken into consideration when burning incense.
355 The single reduction of particles does not mean fewer emissions of gas-phase organics. A



356 comprehensive assessment of incense-burning organics in both gas- and particle-phase should be
357 implemented.

358 Combing pixel-based property estimation and blob identification, the risk assessment analysis of
359 compounds could benefit analysts with less experience with GC×GC. The risk assessment in this
360 work demonstrates that acenaphthylene, dibenzofuran, and PAEs are chemicals of high-risk concern
361 and warrant further control. It was reported that more than half of Chinese residents burn incense
362 every day at home for more than 20 years (Salvi and Apte, 2016). The toxic PAHs detected in indoor
363 air could be 19 times higher than in outdoor air (Salvi and Apte, 2016; Yadav et al., 2022b).
364 Exposure to these hazardous compounds could result in significant health threats. As a result, it is of
365 vital importance to reveal and assess the epidemiological influences of incense burning in future
366 work.

367

368 **Acknowledgment**

369 This research is supported by the National Natural Science Foundation of China (No. 42275104,
370 42107115, 22221004, 41977179), the Natural Science Foundation of Shandong Province, China (No.
371 ZR2021QD111), the Hong Kong Research Grants Council (No. 11304121) and the special fund of
372 State Key Joint Laboratory of Environment Simulation and Pollution Control (No. 22Y01SSPCP).



373 **Reference**

- 374 Ahmad, T., Kenne, L., Olsson, K., and Theander, O.: The formation of 2-furaldehyde and formic acid
375 from pentoses in slightly acidic deuterium oxide studied by ¹H NMR spectroscopy, *Carbohydr Res*,
376 276, 309–320, [https://doi.org/10.1016/0008-6215\(95\)00176-T](https://doi.org/10.1016/0008-6215(95)00176-T), 1995.
- 377 Alam, M. S., Zeraati-Rezaei, S., Liang, Z., Stark, C., Xu, H., MacKenzie, A. R., and Harrison, R. M.:
378 Mapping and quantifying isomer sets of hydrocarbons (\geq C₁₂) in diesel exhaust, lubricating oil and
379 diesel fuel samples using GC \times GC-ToF-MS, *Atmos Meas Tech*, 11, 3047–3058,
380 <https://doi.org/10.5194/amt-11-3047-2018>, 2018.
- 381 Algrim, L. B. and Ziemann, P. J.: Effect of the Keto Group on Yields and Composition of Organic
382 Aerosol Formed from OH Radical-Initiated Reactions of Ketones in the Presence of NO_x, *Journal of*
383 *Physical Chemistry A*, 120, 6978–6989, <https://doi.org/10.1021/acs.jpca.6b05839>, 2016.
- 384 Algrim, L. B. and Ziemann, P. J.: Effect of the Hydroxyl Group on Yields and Composition of Organic
385 Aerosol Formed from OH Radical-Initiated Reactions of Alcohols in the Presence of NO_x, *ACS Earth*
386 *Space Chem*, 3, 413–423, <https://doi.org/10.1021/acsearthspacechem.9b00015>, 2019.
- 387 Bonner, W. A. and Roth1, M. R.: The Conversion of d-Xylose-1-C₁₄ into 2-Furaldehyde- α -C₁₄, *J Am*
388 *Chem Soc*, 81, 5454–5456, <https://doi.org/10.1021/ja01529a051>, 1959.
- 389 Chan, A. W. H., Kautzman, K. E., Chhabra, P. S., Surratt, J. D., Chan, M. N., Crouse, J. D., Kürten, A.,
390 Wennberg, P. O., Flagan, R. C., and Seinfeld, J. H.: Secondary organic aerosol formation from
391 photooxidation of naphthalene and alkylnaphthalenes: Implications for oxidation of intermediate
392 volatility organic compounds (IVOCs), *Atmos Chem Phys*, 9, 3049–3060,
393 <https://doi.org/10.5194/acp-9-3049-2009>, 2009.
- 394 Chan, A. W. H., Chan, M. N., Surratt, J. D., Chhabra, P. S., Loza, C. L., Crouse, J. D., Yee, L. D.,
395 Flagan, R. C., Wennberg, P. O., and Seinfeld, J. H.: Role of aldehyde chemistry and NO_x
396 concentrations in secondary organic aerosol formation, *Atmos Chem Phys*, 10, 7169–7188,
397 <https://doi.org/10.5194/ACP-10-7169-2010>, 2010.
- 398 Charan, S. M., Buenconsejo, R. S., and Seinfeld, J. H.: Secondary organic aerosol yields from the
399 oxidation of benzyl alcohol, *Atmos Chem Phys*, 20, 13167–13190,
400 <https://doi.org/10.5194/acp-20-13167-2020>, 2020.



- 401 Chen, K. S. F., Tsai, Y. P., Lai, C. H., Xiang, Y. K., Chuang, K. Y., and Zhu, Z. H.: Human health-risk
402 assessment based on chronic exposure to the carbonyl compounds and metals emitted by burning
403 incense at temples, *Environmental Science and Pollution Research*, 28, 40640–40652,
404 <https://doi.org/10.1007/S11356-020-10313-1>, 2021a.
- 405 Chen, K. S. F., Tsai, Y. P., Lai, C. H., Xiang, Y. K., Chuang, K. Y., and Zhu, Z. H.: Human health-risk
406 assessment based on chronic exposure to the carbonyl compounds and metals emitted by burning
407 incense at temples, *Environmental Science and Pollution Research*, 28, 40640–40652,
408 <https://doi.org/10.1007/s11356-020-10313-1>, 2021b.
- 409 Depoorter, A., Kalalian, C., Emmelin, C., Lorentz, C., and George, C.: Indoor heterogeneous
410 photochemistry of furfural drives emissions of nitrous acid, *Indoor Air*, 31, 682–692,
411 <https://doi.org/10.1111/INA.12758>, 2021a.
- 412 Depoorter, A., Kalalian, C., Emmelin, C., Lorentz, C., and George, C.: Indoor heterogeneous
413 photochemistry of furfural drives emissions of nitrous acid, *Indoor Air*, 31, 682–692,
414 <https://doi.org/10.1111/ina.12758>, 2021b.
- 415 Drozd, G. T., Zhao, Y., Saliba, G., Frodin, B., Maddox, C., Oliver Chang, M. C., Maldonado, H.,
416 Sardar, S., Weber, R. J., Robinson, A. L., Goldstein, A. H., Chang, M. C. O., Maldonado, H., Sardar, S.,
417 Weber, R. J., Robinson, A. L., Goldstein, A. H., Oliver Chang, M. C., Maldonado, H., Sardar, S.,
418 Weber, R. J., Robinson, A. L., and Goldstein, A. H.: Detailed Speciation of Intermediate Volatility and
419 Semivolatile Organic Compound Emissions from Gasoline Vehicles: Effects of Cold-Starts and
420 Implications for Secondary Organic Aerosol Formation, *Environ Sci Technol*, 53, 1706–1714,
421 <https://doi.org/10.1021/acs.est.8b05600>, 2019.
- 422 Harvey, R. M. and Petrucci, G. A.: Control of ozonolysis kinetics and aerosol yield by nuances in the
423 molecular structure of volatile organic compounds, *Atmos Environ*, 122, 188–195,
424 <https://doi.org/10.1016/j.atmosenv.2015.09.038>, 2015.
- 425 He, X., Zheng, X., You, Y., Zhang, S., Zhao, B., Wang, X., Huang, G., Chen, T., Cao, Y., He, L., Chang,
426 X., Wang, S., and Wu, Y.: Comprehensive chemical characterization of gaseous I/SVOC emissions
427 from heavy-duty diesel vehicles using two-dimensional gas chromatography time-of-flight mass
428 spectrometry, *Environmental Pollution*, 305, 119284, <https://doi.org/10.1016/j.envpol.2022.119284>,



- 429 2022.
- 430 Ho, S. S. H. and Yu, J. Z.: Concentrations of formaldehyde and other carbonyls in environments
431 affected by incense burning, *Journal of Environmental Monitoring*, 4, 728–733,
432 <https://doi.org/10.1039/b200998f>, 2002.
- 433 Huo, Y., Guo, Z., Liu, Y., Wu, D., Ding, X., Zhao, Z., Wu, M., Wang, L., Feng, Y., Chen, Y., Wang, S.,
434 Li, Q., and Chen, J.: Addressing Unresolved Complex Mixture of I/SVOCs Emitted From Incomplete
435 Combustion of Solid Fuels by Nontarget Analysis, *Journal of Geophysical Research: Atmospheres*,
436 126, e2021JD035835, <https://doi.org/10.1029/2021JD035835>, 2021.
- 437 Jetter, J. J., Guo, Z., McBrian, J. A., and Flynn, M. R.: Characterization of emissions from burning
438 incense, *Science of the Total Environment*, 295, 51–67,
439 [https://doi.org/10.1016/S0048-9697\(02\)00043-8](https://doi.org/10.1016/S0048-9697(02)00043-8), 2002.
- 440 Lee, S. C. and Wang, B.: Characteristics of emissions of air pollutants from burning of incense in a
441 large environmental chamber, *Atmos Environ*, 38, 941–951,
442 <https://doi.org/10.1016/j.atmosenv.2003.11.002>, 2004.
- 443 Li, L., Tang, P., Nakao, S., and Cocker, D. R.: Impact of molecular structure on secondary organic
444 aerosol formation from aromatic hydrocarbon photooxidation under low-NO_x conditions, *Atmos*
445 *Chem Phys*, 16, 10793–10808, <https://doi.org/10.5194/acp-16-10793-2016>, 2016.
- 446 Liu, T., Wang, Z., Huang, D. D., Wang, X., and Chan, C. K.: Significant Production of Secondary
447 Organic Aerosol from Emissions of Heated Cooking Oils, *Environ Sci Technol Lett*, 5, 32–37,
448 <https://doi.org/10.1021/acs.estlett.7b00530>, 2018.
- 449 Loza, C. L., Craven, J. S., Yee, L. D., Coggon, M. M., Schwantes, R. H., Shiraiwa, M., Zhang, X.,
450 Schilling, K. A., Ng, N. L., Canagaratna, M. R., Ziemann, P. J., Flagan, R. C., and Seinfeld, J. H.:
451 Secondary organic aerosol yields of 12-carbon alkanes, *Atmos Chem Phys*, 14, 1423–1439,
452 <https://doi.org/10.5194/acp-14-1423-2014>, 2014.
- 453 Lu, F., Li, S., Shen, B., Zhang, J., Liu, L., Shen, X., and Zhao, R.: The emission characteristic of VOCs
454 and the toxicity of BTEX from different mosquito-repellent incenses, *J Hazard Mater*, 384, 121428,
455 <https://doi.org/10.1016/j.jhazmat.2019.121428>, 2020.
- 456 Lu, Q., Zhao, Y., and Robinson, A. L.: Comprehensive organic emission profiles for gasoline, diesel,



457 and gas-turbine engines including intermediate and semi-volatile organic compound emissions, Atmos
458 Chem Phys, 18, 17637–17654, <https://doi.org/10.5194/acp-18-17637-2018>, 2018a.

459 Lu, Q., Zhao, Y., and Robinson, A. L.: Comprehensive organic emission profiles for gasoline, diesel,
460 and gas-turbine engines including intermediate and semi-volatile organic compound emissions, Atmos
461 Chem Phys, 18, 17637–17654, <https://doi.org/10.5194/acp-18-17637-2018>, 2018b.

462 Manoukian, A., Quivet, E., Temime-Roussel, B., Nicolas, M., Maupetit, F., and Wortham, H.:
463 Emission characteristics of air pollutants from incense and candle burning in indoor atmospheres,
464 Environmental Science and Pollution Research, 20, 4659–4670,
465 <https://doi.org/10.1007/s11356-012-1394-y>, 2013.

466 Manoukian, A., Buiron, D., Temime-Roussel, B., Wortham, H., and Quivet, E.: Measurements of
467 VOC/SVOC emission factors from burning incenses in an environmental test chamber: influence of
468 temperature, relative humidity, and air exchange rate, Environmental Science and Pollution Research,
469 23, 6300–6311, <https://doi.org/10.1007/s11356-015-5819-2>, 2016.

470 Matsunaga, A., Docherty, K. S., Lim, Y. B., and Ziemann, P. J.: Composition and yields of secondary
471 organic aerosol formed from OH radical-initiated reactions of linear alkenes in the presence of NO_x:
472 Modeling and measurements, Atmos Environ, 43, 1349–1357,
473 <https://doi.org/10.1016/j.atmosenv.2008.12.004>, 2009.

474 McDonald, B. C., De Gouw, J. A., Gilman, J. B., Jathar, S. H., Akherati, A., Cappa, C. D., Jimenez, J.
475 L., Lee-Taylor, J., Hayes, P. L., McKeen, S. A., Cui, Y. Y., Kim, S. W., Gentner, D. R.,
476 Isaacman-VanWertz, G., Goldstein, A. H., Harley, R. A., Frost, G. J., Roberts, J. M., Ryerson, T. B.,
477 and Trainer, M.: Volatile chemical products emerging as largest petrochemical source of urban organic
478 emissions, Science (1979), 359, 760–764, <https://doi.org/10.1126/science.aaq0524>, 2018.

479 Nabi, D., Gros, J., Dimitriou-Christidis, P., and Arey, J. S.: Mapping environmental partitioning
480 properties of nonpolar complex mixtures by use of GC × GC, Environ Sci Technol, 48, 6814–6826,
481 <https://doi.org/10.1021/es501674p>, 2014.

482 Nimlos, M. R., Qian, X., Davis, M., Himmel, M. E., and Johnson, D. K.: Energetics of xylose
483 decomposition as determined using quantum mechanics modeling, Journal of Physical Chemistry A,
484 110, 11824–11838, <https://doi.org/10.1021/jp0626770>, 2006.



- 485 Salvi, S. and Apte, K.: Household air pollution and its effects on health, *F1000Res*, 5,
486 <https://doi.org/10.12688/f1000research.7552.1>, 2016.
- 487 Shah, R. U., Coggon, M. M., Gkatzelis, G. I., McDonald, B. C., Tasoglou, A., Huber, H., Gilman, J.,
488 Warneke, C., Robinson, A. L., and Presto, A. A.: Urban Oxidation Flow Reactor Measurements Reveal
489 Significant Secondary Organic Aerosol Contributions from Volatile Emissions of Emerging
490 Importance, *Environ Sci Technol*, 54, 714–725, <https://doi.org/10.1021/acs.est.9b06531>, 2020.
- 491 Shang, X., Pan, H., Li, M., Miao, X., and Ding, H.: *Lonicera japonica* Thunb.: Ethnopharmacology,
492 phytochemistry and pharmacology of an important traditional Chinese medicine,
493 <https://doi.org/10.1016/j.jep.2011.08.016>, 2011.
- 494 Silva, G. V., Martins, A. O., and Martins, S. D. S.: Indoor air quality: Assessment of dangerous
495 substances in incense products, *Int J Environ Res Public Health*, 18,
496 <https://doi.org/10.3390/ijerph18158086>, 2021.
- 497 Song, K., Guo, S., Gong, Y., Lv, D., Zhang, Y., Wan, Z., Li, T., Zhu, W., Wang, H., Yu, Y., Tan, R.,
498 Shen, R., Lu, S., Li, S., Chen, Y., and Hu, M.: Impact of cooking style and oil on semi-volatile and
499 intermediate volatility organic compound emissions from Chinese domestic cooking, *Atmos Chem*
500 *Phys*, 22, 9827–9841, <https://doi.org/10.5194/ACP-22-9827-2022>, 2022a.
- 501 Song, K., Gong, Y., Guo, S., Lv, D., Wang, H., Wan, Z., Yu, Y., Tang, R., Li, T., Tan, R., Zhu, W., Shen,
502 R., and Lu, S.: Investigation of partition coefficients and fingerprints of atmospheric gas- and
503 particle-phase intermediate volatility and semi-volatile organic compounds using pixel-based
504 approaches, *J Chromatogr A*, 1665, 462808, <https://doi.org/10.1016/j.chroma.2022.462808>, 2022b.
- 505 Song, K., Guo, S., Gong, Y., Lv, D., Wan, Z., Zhang, Y., Fu, Z., Hu, K., and Lu, S.: Non-target scanning
506 of organics from cooking emissions using comprehensive two-dimensional gas chromatography-mass
507 spectrometer (GC×GC-MS), *Applied Geochemistry*, 151,
508 <https://doi.org/10.1016/j.apgeochem.2023.105601>, 2023.
- 509 Staub, P. O., Schiestl, F. P., Leonti, M., and Weckerle, C. S.: Chemical analysis of incense smokes used
510 in Shaxi, Southwest China: A novel methodological approach in ethnobotany, *J Ethnopharmacol*, 138,
511 212–218, <https://doi.org/10.1016/j.jep.2011.08.078>, 2011.
- 512 Stewart, G. J., Nelson, B. S., Acton, W. J. F., Vaughan, A. R., Hopkins, J. R., Yunus, S. S. M., Hewitt, C.



513 N., Nemitz, E., Mandal, T. K., Gadi, R., Sahu, Lokesh. K., Rickard, A. R., Lee, J. D., and Hamilton, J.
514 F.: Comprehensive organic emission profiles, secondary organic aerosol production potential, and OH
515 reactivity of domestic fuel combustion in Delhi, India, *Environmental Science: Atmospheres*, 1, 104–
516 117, <https://doi.org/10.1039/d0ea00009d>, 2021.

517 Suzuki, S., Kiuchi, S., Kinoshita, K., Takeda, Y., Sakaida, S., Konno, M., Tanaka, K., and Oguma, M.:
518 Formation of polycyclic aromatic hydrocarbons, benzofuran, and dibenzofuran in fuel-rich oxidation
519 of toluene using a flow reactor, *Physical Chemistry Chemical Physics*, 23,
520 <https://doi.org/10.1039/d0cp06615j>, 2021.

521 Tang, R., Lu, Q., Guo, S., Wang, H., Song, K., Yu, Y., Tan, R., Liu, K., Shen, R., Chen, S., Zeng, L.,
522 Jorga, S. D., Zhang, Z., Zhang, W., Shuai, S., and Robinson, A. L.: Measurement report: Distinct
523 emissions and volatility distribution of intermediate-volatility organic compounds from on-road
524 Chinese gasoline vehicles: Implication of high secondary organic aerosol formation potential, *Atmos*
525 *Chem Phys*, 21, 2569–2583, <https://doi.org/10.5194/acp-21-2569-2021>, 2021a.

526 Tang, R., Lu, Q., Guo, S., Wang, H., Song, K., Yu, Y., Tan, R., Liu, K., Shen, R., Chen, S., Zeng, L.,
527 Jorga, S. D., Zhang, Z., Zhang, W., Shuai, S., and Robinson, A. L.: Measurement report: Distinct
528 emissions and volatility distribution of intermediate-volatility organic compounds from on-road
529 Chinese gasoline vehicles: Implication of high secondary organic aerosol formation potential, *Atmos*
530 *Chem Phys*, 21, 2569–2583, <https://doi.org/10.5194/acp-21-2569-2021>, 2021b.

531 Tkacik, D. S., Presto, A. A., Donahue, N. M., and Robinson, A. L.: Secondary organic aerosol
532 formation from intermediate-volatility organic compounds: Cyclic, linear, and branched alkanes,
533 *Environ Sci Technol*, 46, 8773–8781, <https://doi.org/10.1021/es301112c>, 2012.

534 Tran, T. C. and Marriott, P. J.: Characterization of incense smoke by solid phase
535 microextraction-Comprehensive two-dimensional gas chromatography (GC×GC), *Atmos Environ*, 41,
536 5756–5768, <https://doi.org/10.1016/j.atmosenv.2007.02.030>, 2007.

537 Uhde, E. and Salthammer, T.: Impact of reaction products from building materials and furnishings on
538 indoor air quality-A review of recent advances in indoor chemistry, *Atmos Environ*, 41, 3111–3128,
539 <https://doi.org/10.1016/j.atmosenv.2006.05.082>, 2007.

540 Wang, J., Jin, L., Gao, J., Shi, J., Zhao, Y., Liu, S., Jin, T., Bai, Z., and Wu, C. Y.: Investigation of



541 speciated VOC in gasoline vehicular exhaust under ECE and EUDC test cycles, *Science of the Total*
542 *Environment*, 445–446, 110–116, <https://doi.org/10.1016/j.scitotenv.2012.12.044>, 2013.

543 Wang, Y. and Qian, H.: Phthalates and their impacts on human health,
544 <https://doi.org/10.3390/healthcare9050603>, 2021.

545 Wong, A., Lou, W., Ho, K. fai K., Yiu, B. K. fung, Lin, S., Chu, W. C. wing, Abrigo, J., Lee, D., Lam,
546 B. Y. ka, Au, L. W. chi, Soo, Y. O. yan, Lau, A. Y. lun, Kwok, T. C. yui, Leung, T. W. hong, Lam, L. C.
547 wa, Ho, K. fai K., and Mok, V. C. tong: Indoor incense burning impacts cognitive functions and brain
548 functional connectivity in community older adults, *Sci Rep*, 10, 1–11,
549 <https://doi.org/10.1038/s41598-020-63568-6>, 2020.

550 Wu, W., Zhao, B., Wang, S., and Hao, J.: Ozone and secondary organic aerosol formation potential
551 from anthropogenic volatile organic compounds emissions in China, *J Environ Sci (China)*, 53, 224–
552 237, <https://doi.org/10.1016/j.jes.2016.03.025>, 2017.

553 Yadav, V. K., Malik, P., Tirth, V., Khan, S. H., Yadav, K. K., Islam, S., Choudhary, N., Inwati, G. K.,
554 Arabi, A., Kim, D. H., and Jeon, B. H.: Health and Environmental Risks of Incense Smoke:
555 Mechanistic Insights and Cumulative Evidence, *J Inflamm Res*, 15, 2665–2693,
556 <https://doi.org/10.2147/JIR.S347489>, 2022a.

557 Yadav, V. K., Malik, P., Tirth, V., Khan, S. H., Yadav, K. K., Islam, S., Choudhary, N., Inwati, G. K.,
558 Arabi, A., Kim, D. H., and Jeon, B. H.: Health and Environmental Risks of Incense Smoke:
559 Mechanistic Insights and Cumulative Evidence, *J Inflamm Res*, 15, 2665–2693,
560 <https://doi.org/10.2147/JIR.S347489>, 2022b.

561 Yang, T. T., Lin, T. S., and Chang, M.: Characteristics of emissions of volatile organic compounds
562 from smoldering incense, *Bull Environ Contam Toxicol*, 78, 308–313,
563 <https://doi.org/10.1007/s00128-007-9184-9>, 2007.

564 Yang, T. T., Ho, S. C., Chuang, L. te, Chuang, H. C., Li, Y. T., and Wu, J. J.: Characterization of
565 particulate-phase polycyclic aromatic hydrocarbons emitted from incense burning and their
566 bioreactivity in RAW264.7 macrophage, *Environmental Pollution*, 220, 1190–1198,
567 <https://doi.org/10.1016/j.envpol.2016.11.016>, 2017.

568 Yu, Y., Guo, S., Wang, H., Shen, R., Zhu, W., Tan, R., Song, K., Zhang, Z., Li, S., Chen, Y., and Hu, M.:



569 Importance of Semivolatile/Intermediate-Volatility Organic Compounds to Secondary Organic
570 Aerosol Formation from Chinese Domestic Cooking Emissions, *Environ Sci Technol Lett*,
571 <https://doi.org/10.1021/acs.estlett.2c00207>, 2022.

572 Yue, T., Yue, X., Chai, F., Hu, J., Lai, Y., He, L., and Zhu, R.: Characteristics of volatile organic
573 compounds (VOCs) from the evaporative emissions of modern passenger cars, *Atmos Environ*, 151,
574 62–69, <https://doi.org/10.1016/j.atmosenv.2016.12.008>, 2017.

575 Zhao, Y., Hu, M., Slanina, S., and Zhang, Y.: Chemical compositions of fine particulate organic matter
576 emitted from Chinese cooking, *Environ Sci Technol*, 41, 99–105, <https://doi.org/10.1021/es0614518>,
577 2007.

578 Zhao, Y., Hennigan, C. J., May, A. A., Tkacik, D. S., De Gouw, J. A., Gilman, J. B., Kuster, W. C.,
579 Borbon, A., and Robinson, A. L.: Intermediate-volatility organic compounds: A large source of
580 secondary organic aerosol, *Environ Sci Technol*, 48, 13743–13750, <https://doi.org/10.1021/es5035188>,
581 2014a.

582 Zhao, Y., Hennigan, C. J., May, A. A., Tkacik, D. S., de Gouw, J. A., Gilman, J. B., Kuster, W. C.,
583 Borbon, A., and Robinson, A. L.: Intermediate-volatility organic compounds: A large source of
584 secondary organic aerosol, *Environ Sci Technol*, 48, 13743–13750, <https://doi.org/10.1021/es5035188>,
585 2014b.

586 Zhao, Y., Nguyen, N. T., Presto, A. A., Hennigan, C. J., May, A. A., and Robinson, A. L.: Intermediate
587 Volatility Organic Compound Emissions from On-Road Diesel Vehicles: Chemical Composition,
588 Emission Factors, and Estimated Secondary Organic Aerosol Production, *Environ Sci Technol*, 49,
589 11516–11526, <https://doi.org/10.1021/acs.est.5b02841>, 2015.

590 Zhao, Y., Saleh, R., Saliba, G., Presto, A. A., Gordon, T. D., Drozd, G. T., Goldstein, A. H., Donahue,
591 N. M., and Robinson, A. L.: Reducing secondary organic aerosol formation from gasoline vehicle
592 exhaust, *Proc Natl Acad Sci U S A*, 114, 6984–6989, <https://doi.org/10.1073/pnas.1620911114>, 2017.

593 Zhu, X., Han, Y., Feng, Y., Cheng, P., Peng, Y., Wang, J., Cai, J., and Chen, Y.: Formation and emission
594 characteristics of intermediate volatile organic compounds (IVOCs) from the combustion of biomass
595 and their cellulose, hemicellulose, and lignin, *Atmos Environ*, 286, 119217,
596 <https://doi.org/10.1016/j.atmosenv.2022.119217>, 2022.



597 Zushi, Y., Yamatori, Y., Nagata, J., and Nabi, D.: Comprehensive two-dimensional
598 gas-chromatography-based property estimation to assess the fate and behavior of complex mixtures: A
599 case study of vehicle engine oil, *Science of the Total Environment*, 669, 739–745,
600 <https://doi.org/10.1016/j.scitotenv.2019.03.157>, 2019.
601



602 **Figures**

603 **Figure 1.** Volatility distributions of EF, OFP, and SOA with chemical class in each volatility bin. The
604 x -axis is the unsaturated vapor concentration in logarithmic form ($\log C^*$, $\mu\text{g m}^{-3}$). The y -axis is the
605 normalized mass emission factor (100%).

606 **Figure 2.** Positive (a) and negative loadings (b) of incense burning samples describing similarities
607 and differences between chromatograms. The color bar is the loading.

608 **Figure 3.** Chemicals with high bioaccumulation potential (BAP) assessed by pixel-based approaches.

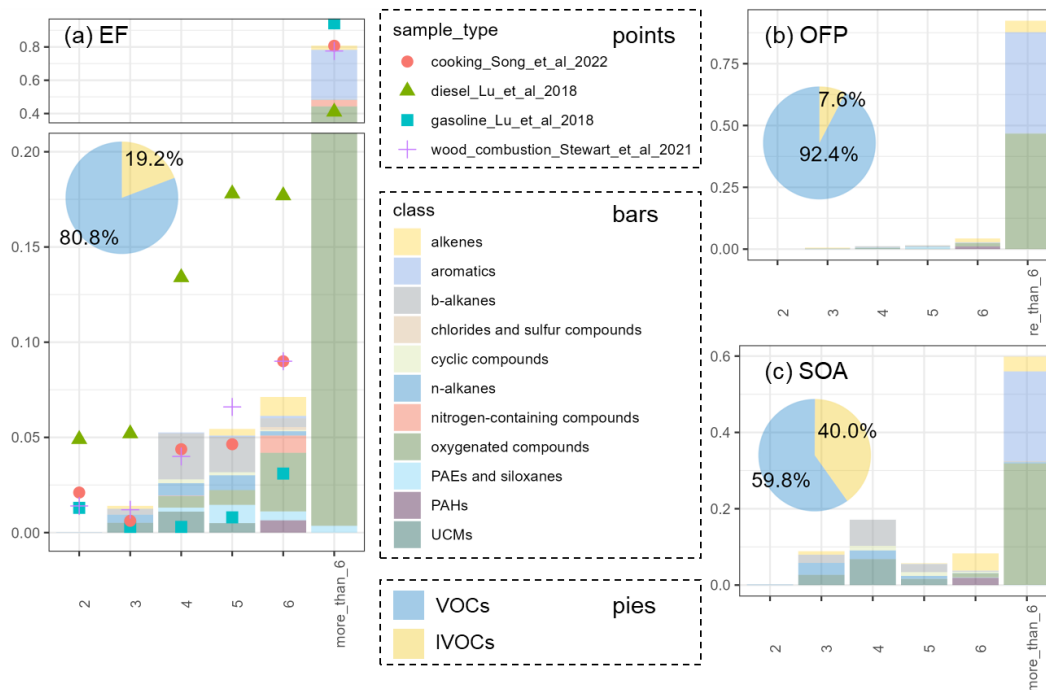
609

610

611



612

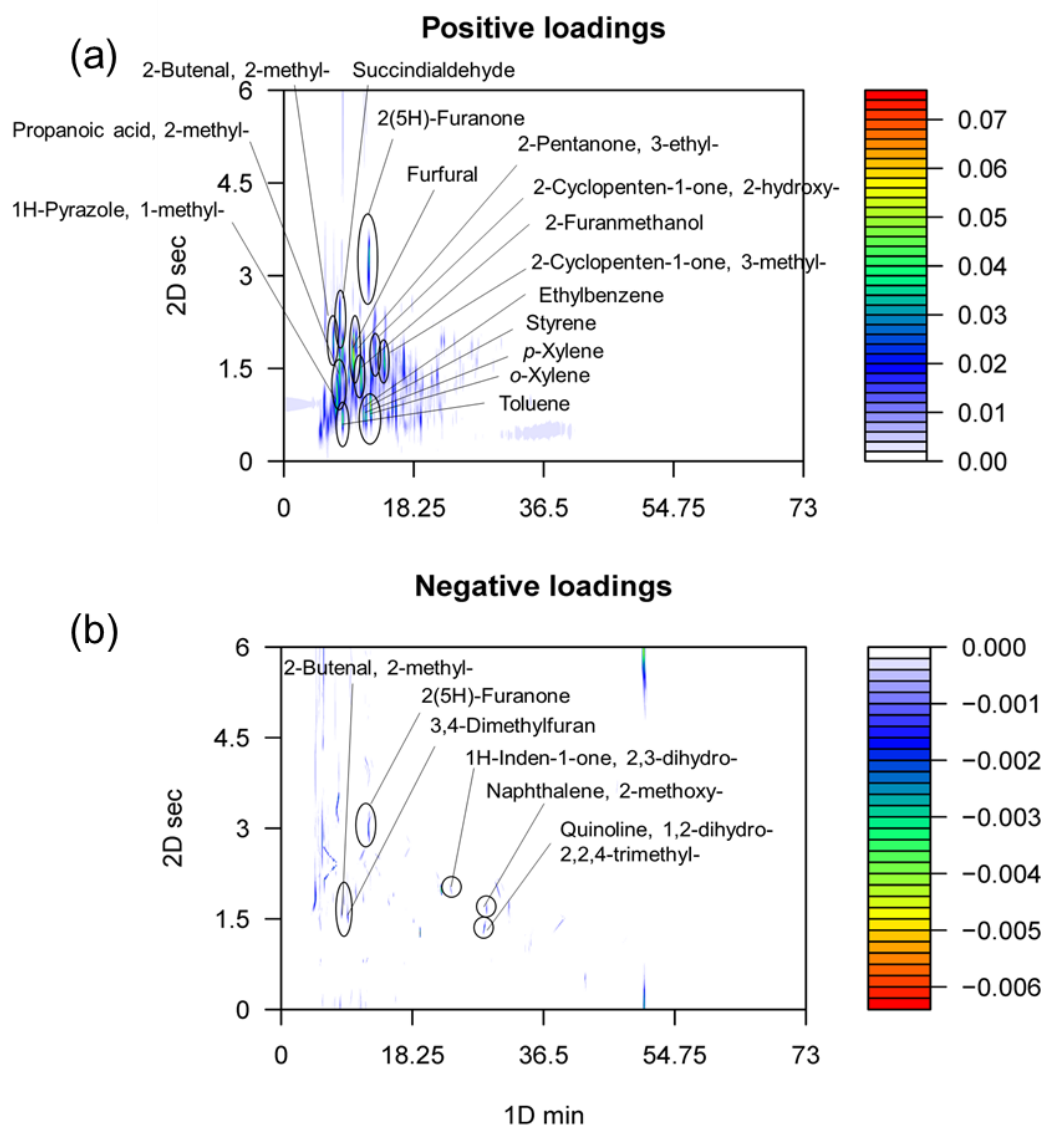


613

614 **Figure 1.** Volatility distributions of EF, OFP, and SOA with chemical class in each volatility bin. The

615 x -axis is the unsaturated vapor concentration in logarithmic form ($\log C^*$, $\mu\text{g m}^{-3}$). The y -axis is the

616 normalized mass emission factor (100%).

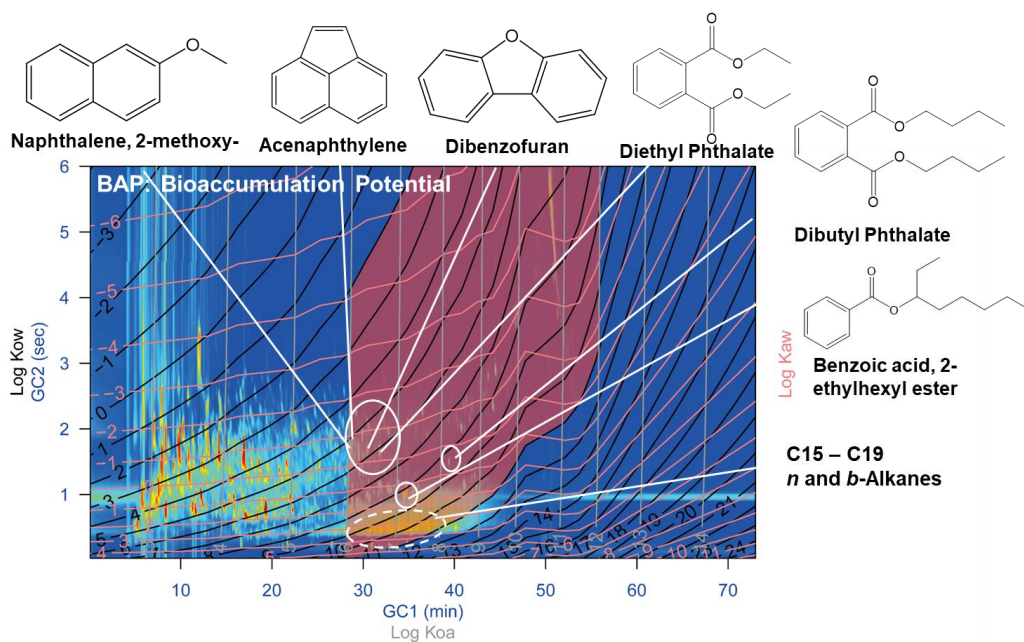


617

618 **Figure 2.** Positive (a) and negative loadings (b) of incense burning samples describing similarities

619 and differences between chromatograms. The color bar is the loading.

620



621

622 **Figure 3.** Chemicals with high bioaccumulation potential (BAP) assessed by pixel-based approaches.

623